The Helicity Issue in Large Scale Dynamos

Axel Brandenburg

NORDITA, Blegdamsvej 17, DK-2100 Copenhagen Ø, Denmark

Abstract. The connection between helically isotropic MHD turbulence and mean-field dynamo theory is reviewed. The nonlinearity in the mean-field theory is not yet well established, but detailed comparison with simulations begin to help select viable forms of the nonlinearity. The crucial discriminant is the magnetic helicity, which is known to evolve only on a slow resistive time scale in the limit of large magnetic Reynolds number. Particular emphasis is put on the possibility of memory effects, which means that an additional explicitly time-dependent equation for the nonlinearity is solved simultaneously with the mean-field equations. This approach leads to better agreement with the simulations, while it would also produce more favorable agreement between models and stellar dynamos.

1 Introduction

In an early paper Parker [1] identified cyclonic convection as a key process for converting large scale toroidal magnetic field into poloidal fields that have coherence over about half a hemisphere. This process is now generally referred to as the α-effect, although it may arise not only from thermal buoyancy [2], but also from magnetic buoyancy [3,4,5], the magneto-rotational instability [6,7], or some other magnetic instability [8]. In each case the effect of the Coriolis force together with some kind of radial stratification is crucial for making the motions helical [9]. Upward moving fluid expands, and the Coriolis force makes it rotate retrograde, causing negative (positive) kinetic helicity in the northern (southern) hemisphere. Downward moving fluid contracts, rotates in the prograde direction and contributes in the same sense to negative (positive) kinetic helicity on the northern (southern) hemisphere. This causes a positive α-effect in the northern hemisphere, but if magnetic stresses and shear become strong (for example in accretion discs) the sign may reverse [10,11].

When combined with differential rotation, the main outcome of α-effect models is the possibility of cyclic magnetic fields associated with latitudinal migration. The first global (two-dimensional) models were presented by Steenbeck & Krause [12], but similar models, with different physics, are still being studied today [13,14,15]. The migratory behavior is best seen in contours of the longitudinally averaged mean magnetic field versus latitude and time, which should show tilted structures converging to the equator. Such plots can be compared with the solar butterfly diagram of sunspot numbers (so called because the structures resemble a sequence of butterflies).

E. Falgarone and T. Passot (Eds.): LNP 614, pp. 402–431, 2003.

A key property of all these models is that not only the motions are helical, but the large scale magnetic field itself is also helical. Of course, not all dynamos require helicity, but nonhelical dynamos tend to generate preferentially small-scale fields [16]. In a recent attempt, Vishniac & Cho [17] proposed a mechanism relevant in particular to accretion discs where shear is strong. Their mechanism would not lead to the production of net magnetic helicity, but numerical simulations [18] failed so far to show convincingly *large scale* dynamo action based on the proposed mechanism. Shear does produce large scale fields, but only in the toroidal direction. It does not explain the latitudinal coherence of the field over several tens of degrees (corresponding to several hundred megameters). On the other hand, there is direct observational evidence that the solar magnetic field is indeed helical. (We shall return to observations in Sect. 2.)

The trouble with helical fields is that magnetic helicity is conserved by the induction equation in the ideal limit and can only change on a resistive time scale, provided there is no significant loss through boundaries (at the surface or the equator, for example). This approximate magnetic helicity conservation leads to magnetic field saturation on a resistive time scale [19]. Depending on how effectively the boundaries transmit magnetic energy and helicity, the final saturation amplitude will be lowered if losses occur preferentially on large scales while the (linear) growth rate of magnetic energy (past initial saturation) remains *unchanged* [20]. In this sense final saturation can be achieved earlier. The above results are particularly clear when the flow is nearly fully helical, i.e. when the normalized kinetic helicity, $\epsilon_{\rm f} \equiv \langle \boldsymbol{\omega} \cdot \mathbf{u} \rangle / (\omega_{\rm rms} u_{\rm rms})$, where $\boldsymbol{\omega} = \boldsymbol{\nabla} \times \mathbf{u}$ is the vorticity, is large. In the sun, and probably in all other celestial bodies with rotating turbulence, the relative kinetic helicity is small; $\epsilon_{\rm f} \sim 5\%$. It is however this small helical fraction of the turbulence that is responsible for the a finite but small α-effect, so a proper understanding of its dynamics is crucial if one wants to build models based on the α-effect. Below we shall also discuss the alternative that astrophysical dynamos may shed preferentially small-scale helical fields through the boundaries. This could theoretically enhance large-scale dynamo action [21,22,23].

2 Magnetic Helicity Production

Before we begin discussing the magnetic helicity problem and possible remedies we need to be sure that the solar dynamo is indeed likely to involve significant amounts of magnetic helicity. There is direct observational evidence that the field of the sun is actually helical. Firstly, active regions are known to have systematically different signs of current helicity in the two hemispheres [24,25,26,27]; preferentially negative (positive) in the northern (southern) hemisphere. Secondly, magnetic helicity flux from the solar surface has also been inferred and this confirms the same sign as that of the current helicity. The magnetic helicity flux driven by the surface differential rotation has been estimated by Berger & Ruzmaikin [28], who find a total magnetic helicity flux on the order of $4 \times 10^{46}\,{\rm Mx}^2$ over the 22 year solar cycle. Similar values were also found by DeVore [29].

Finally, Chae [30] estimated the magnetic helicity flux based on counting the crossings of pairs of flux tubes. Combined with the assumption that two nearly aligned flux tubes are nearly parallel (rather than antiparallel) his results again suggest that the magnetic helicity is preferentially negative (positive) in the northern (southern) hemisphere.

The magnetic helicity is noisy, i.e. the sign can fluctuate and has only on average systematic behavior. This reflects the fact that only a fraction of the turbulence is helical. Thus, detailed understanding and measurements of the departures from systematic behavior is just as important as understanding and recording the systematic behavior.

In astrophysical flows, kinetic helicity can be generated in rotating stratified turbulence [9]. Such flows are intrinsically anisotropic. Whilst this is not a problem for numerical simulations, it definitely complicates the theoretical understanding and one should not be surprised if some fundamental aspects of mean-field theory (e.g. α proportional to $-\langle\boldsymbol{\omega}\cdot\mathbf{u}\rangle$) are not recovered. We just mention that under certain conditions, stratified rotating flows exhibit an α-tensor whose vertical (z-z) component has the opposite sign as the horizontal (x-x and y-y) components [32,33,34,35].)

In the following we concentrate on the isotropic helical aspects of the turbulence. This is accomplished by driving the flow with random polarized waves in a periodic domain. In most of the cases we use fully helical turbulence, but in many estimates the fraction of helicity enters only as an additional scaling factor [23]. The main goal here is a better understanding of the α-effect and the nonlinear feedback when the field becomes dynamically important. We therefore discuss in detail the perhaps simplest possible system: the α^2-dynamo in a periodic box.

In spherical geometry, the term α^2-dynamo refers to the fact that both large-scale poloidal and toroidal fields are maintained against ohmic decay by the α-effect. By contrast, the $\alpha\Omega$-dynamo is one where the large-scale toroidal field is generated mostly by differential rotation (the Ω-effect) and the α-effect can be neglected by comparison. If the α-effect is not neglected one speaks of an $\alpha^2\Omega$-dynamo. We stress that the α^2-dynamo has nothing to do with the so-called small-scale dynamo. These are turbulent dynamos operating only on scales less than the energy-carrying scale of the turbulence. They are quite common if the flows are non-helical. By contrast, both α^2 and $\alpha\Omega$-dynamos also generate fields on large scales, but they are necessarily accompanied by some level of small scale fields as well.

In its simplest form the α^2-dynamo equations for isotropic α and turbulent diffusivity $\eta_{\rm t}$ can be written as

$$\frac{\partial\overline{\mathbf{B}}}{\partial t}=\boldsymbol{\nabla}\times\left(\alpha\overline{\mathbf{B}}-\eta_{\rm T}\mu_0\overline{\mathbf{J}}\right), \tag{1}$$

where $\overline{\mathbf{J}}=\boldsymbol{\nabla}\times\overline{\mathbf{B}}/\mu_0$ is the mean current density and μ_0 is the magnetic permeability. This equation permits plane wave solutions of the form $\overline{\mathbf{B}}=\hat{\mathbf{B}}\exp(\lambda t+{\rm i}\boldsymbol{k}\cdot\boldsymbol{x})$, with the dispersion relation $\lambda=\pm|\alpha|k-\eta_{\rm T}k^2$, where $k=|\boldsymbol{k}|$.

The maximum of λ is where $\mathrm{d}\lambda/\mathrm{d}k = 0$, which yields

$$k = k_{\max} = \alpha/(2\eta_{\mathrm{T}}). \tag{2}$$

For a periodic box of size L^3, the most easily excited mode has $k = k_1 \equiv 2\pi/L$, and the $\boldsymbol{k}$ vector can point in any of the three coordinate directions. For $\alpha < 0$ (the case considered in [19]), the three possible eigenfunctions are

$$\mathbf{B}^{(z)} = B_0 \begin{pmatrix} \cos k_1 z \\ \sin k_1 z \\ 0 \end{pmatrix}, \quad \mathbf{B}^{(x)} = B_0 \begin{pmatrix} 0 \\ \cos k_1 x \\ \sin k_1 x \end{pmatrix}, \quad \mathbf{B}^{(y)} = B_0 \begin{pmatrix} \sin k_1 y \\ 0 \\ \cos k_1 y \end{pmatrix}, \tag{3}$$

where we have ignored arbitrary phase shifts in any of the three directions. All three solutions have been found in the simulations [19].

In the simulations there is of course no explicit α-effect in the usual sense, because we just solve the primitive MHD equations. The turbulence does, however, display *collective behavior* – just as it is expected based on mean-field α^2-dynamo theory, as explained above. We begin with the simulations.

3 Helical Turbulence: Prototype of an α^2-Dynamo

We consider a compressible isothermal gas with constant sound speed c_{s}, constant dynamical viscosity μ, and constant magnetic diffusivity η. To make sure the magnetic field stays solenoidal, i.e. $\boldsymbol{\nabla} \cdot \mathbf{B} = 0$, we express $\mathbf{B}$ in terms of the magnetic vector potential $\mathbf{A}$, so the field is written as $\mathbf{B} = \boldsymbol{\nabla} \times \mathbf{A}$. The governing equations for density ρ, velocity $\mathbf{u}$, and magnetic vector potential $\mathbf{A}$, are given by

$$\frac{\mathrm{D} \ln \rho}{\mathrm{D}t} = -\boldsymbol{\nabla} \cdot \mathbf{u}, \tag{4}$$

$$\frac{\mathrm{D}\mathbf{u}}{\mathrm{D}t} = -c_{\mathrm{s}}^2 \boldsymbol{\nabla} \ln \rho + \frac{\mathbf{J} \times \mathbf{B}}{\rho} + \frac{\mu}{\rho}(\nabla^2 \mathbf{u} + \tfrac{1}{3} \boldsymbol{\nabla} \boldsymbol{\nabla} \cdot \mathbf{u}) + \boldsymbol{f}, \tag{5}$$

$$\frac{\partial \mathbf{A}}{\partial t} = \mathbf{u} \times \mathbf{B} - \eta \mu_0 \mathbf{J} - \boldsymbol{\nabla} \phi, \tag{6}$$

where $\mathrm{D}/\mathrm{D}t = \partial/\partial t + \mathbf{u} \cdot \boldsymbol{\nabla}$ is the advective derivative. The current density, $\mathbf{J} = \boldsymbol{\nabla} \times \mathbf{B}/\mu_0$, is obtained in the form $\mu_0 \mathbf{J} = -\nabla^2 \mathbf{A} + \boldsymbol{\nabla} \boldsymbol{\nabla} \cdot \mathbf{A}$. We often use $\phi = 0$ as a convenient gauge for the electrostatic potential. Other frequent choices are $\phi = -\eta \boldsymbol{\nabla} \cdot \mathbf{A}$, $\phi = \mathbf{u} \cdot \mathbf{A}$, or combinations of these [36]. The Coulomb gauge, $\boldsymbol{\nabla} \cdot \mathbf{A} = 0$, corresponds to $\phi = -\boldsymbol{\nabla} \cdot \mathbf{E}$, where $\mathbf{E} = -\mathbf{u} \times \mathbf{B} + \eta \mu_0 \mathbf{J}$, but the original reason for solving for $\mathbf{A}$ instead of $\mathbf{B}$ was just to get rid of the solenoidality condition, so the Coulomb condition has computational disadvantages.

For the following it is useful to recall that each vector field can be decomposed into a solenoidal and two vortical parts with positive and negative helicity, respectively. These are also referred to as Chandrasekhar-Kendall functions. Although it is often useful to decompose the magnetic field into positive and negative helical parts, we also use the helical fields (with positive helicity) as forcing

function $\boldsymbol{f}$ of the flow. We restrict ourselves to functions selected from a finite band of wavenumbers around the wavenumber $k_{\rm f}$, but direction and amplitude are chosen randomly at each timestep. Details can be found in [19]. Similar work was first carried out by Meneguzzi et al. [37], but at the time one was barely able to run even until saturation. Throughout the nineties, work has been done on forced ABC flows [38,39,40]. In none of these investigations, however, the issue of resistively slow magnetic helicity evolution past initial saturation has been noted. It is exactly this aspect that has now become so crucial in understanding the saturation behavior of nonlinear dynamos. We begin by discussing first the linear (kinematic) evolution of the magnetic field.

3.1 Linear Behavior

If the magnetic Reynolds number, defined here as $R_{\rm m} = u_{\rm rms}/(\eta k_{\rm f})$, exceeds a certain critical value, $R_{\rm m}^{\rm (crit)}$, there is dynamo action. For helical flows, the so defined $R_{\rm m}^{\rm (crit)}$ is between 1 and 2 (see Table 1 of [19]). In the supercritical case, $R_{\rm m} > R_{\rm m}^{\rm (crit)}$, the field grows exponentially with growth rate λ, which scales with the inverse turnover time, $u_{\rm rms}/k_{\rm f}$. The resistively limited saturation behavior that will be discussed below in full detail has no obvious correspondence in the kinematic stage when the field is too weak to affect the motions by the Lorentz force [41]. Nevertheless, there is actually a subtle effect on the shape of the eigenfunction as $R_{\rm m}$ increases. Before we can appreciate this, we need to discuss the effect the kinetic helicity has on the field.

A helical velocity tends to drive helicity in the magnetic field as well, but in the nonresistive limit magnetic helicity conservation dictates that $\langle \mathbf{A} \cdot \mathbf{B} \rangle = {\rm const} = 0$ if the initial field (or at least its helicity) was infinitesimally weak. Thus, there must be some kind of magnetic helicity cancelation. Under homogeneous isotropic conditions there cannot be a spatial segregation in positive and negative helical parts. Instead, there is a spectral segregation: there is a bump at the forcing wavenumber and another 'secondary' bump at somewhat smaller wavenumber. The two bumps have opposite sign of magnetic helicity such that the net magnetic helicity is zero. At the forcing wavenumber, the sign of magnetic helicity agrees with that of the kinetic helicity, but at smaller wavenumber the sign of magnetic helicity is opposite. At small $R_{\rm m}$, this secondary peak can be identified with the wavenumber where the corresponding α^2-dynamo has maximum growth rate; see (2). Simulations show that as $R_{\rm m}$ increases, $k_{\rm max}$ approaches $\frac{1}{2}k_{\rm f}$ [23]. This agrees qualitatively with earlier results [41,42] which suggested that the magnetic helicity approaches zero in the high-$R_{\rm m}$ limit.

3.2 Nonlinear Behavior

Eventually, the magnetic energy stops increasing exponentially. This is due to the nonlinear terms, in particular the Lorentz force $\mathbf{J} \times \mathbf{B}$ in (5), which begins to affect the velocity field. The temporal growth of the power spectra saturates, but only partially; see Fig. 1, where we show data from a run with forcing at

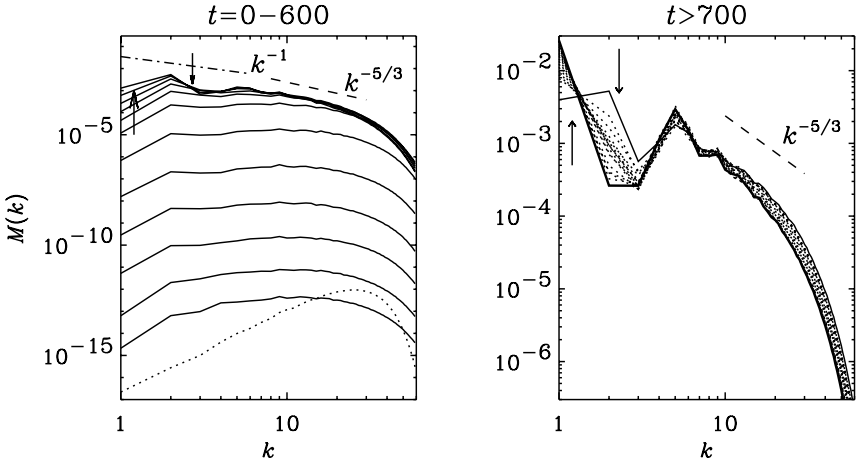

Fig. 1. Power spectra of magnetic energy of Run 3 of [19]. During the initial growth phase the field saturates at small scales first and only later at large scales (left hand panel). Later, when also the large scale field saturates, the field at intermediate scales ($k = 2$, 3, and 4) becomes suppressed. In the second panel, intermediate times are shown as dotted lines, $t = 700$ is shown in solid and $t = 1600$ is shown as a thick solid line. The forcing wavenumber is $k_\mathrm{f} = 5$.

wavenumber $k_\mathrm{f} = 5$. In the left hand panel we see that by the time $t = 600$ the power spectra have saturated at larger wavenumbers, $k \gtrsim 3$. It takes until $t \simeq 1600$ for the power spectra to be saturated also at $k = 1$ (right hand panel of Fig. 1). In order to see more clearly the behavior at large scales, we show in Fig. 2 data from a run with $k_\mathrm{f} = 27$ and compare spectra in the linear and nonlinear regimes. In the linear regime, all spectra are just shifted along the ordinate, so the spectra have been compensated by the factor $M_\mathrm{ini} \exp(2\lambda t)$, where λ is the growth rate and M_ini the initial magnetic energy. In the nonlinear regime the bump on the right stays at approximately the same wavenumber (the forcing wavenumber), while the bump on the left propagates gradually further to the left. As it does so, and since the amplitude of the secondary peak even increases slightly, the net magnetic helicity inevitably increases (or rather becomes more negative in the present case). But because of the asymptotic magnetic helicity conservation, this can only happen on a slow resistive time scale. This leads to the appearance of a (resistively) slow saturation phase past the initial saturation; see Fig. 3.

3.3 The Final Saturation Value

In a periodic box with helically driven turbulence, the final saturation value of the magnetic field is determined by the ratio of the size of the domain to the scale

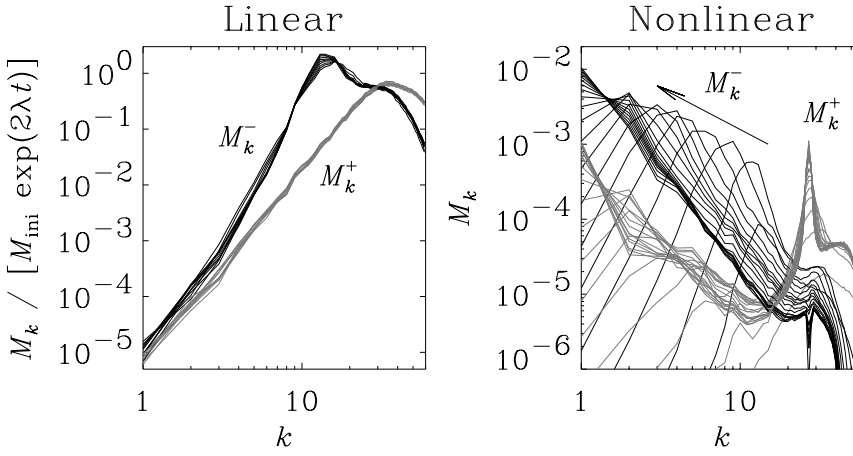

Fig. 2. Power spectra of magnetic energy of positively and negatively polarized parts (M_k^+ and M_k^-) in the linear and nonlinear regimes. The spectra in the linear regime have been compensated by the exponential growth factor to make them collapse on top of each other. Here the forcing wavenumber is in the dissipative subrange, $k_{\rm f} = 27$, but this allows enough scale separation to see the inverse transfer of magnetic energy to smaller k. The data are from Run B of [44].

of the forcing. This is best seen by considering the magnetic helicity equation

$$\frac{\mathrm{d}}{\mathrm{d}t}\langle \mathbf{A}\cdot\mathbf{B}\rangle = -2\eta\mu_0\langle \mathbf{J}\cdot\mathbf{B}\rangle. \tag{7}$$

If $\langle \mathbf{A}\cdot\mathbf{B}\rangle$ were not gauge invariant (for example if there are open boundaries), (7) would be useless. In particular, $\langle \mathbf{A}\cdot\mathbf{B}\rangle$ will in general not be constant in the steady state (see Fig. 2 of [23], for an example). One therefore has to go to the gauge-invariant relative magnetic helicity of Berger & Field [43]. This has been done in [20,23]. In the present case of periodic boundaries, however, $\langle \mathbf{A}\cdot\mathbf{B}\rangle$ is automatically gauge invariant and therefore a physically meaningful quantity, so it must be constant in the steady state. Equation (7) says that then the current helicity, $\langle \mathbf{J}\cdot\mathbf{B}\rangle$, must vanish. At first glance this seems to be in conflict with the idea of building up a helical large scale field. The solution is that there must then be an equal amount of small scale current helicity so that

$$\langle \mathbf{J}\cdot\mathbf{B}\rangle = \langle \overline{\mathbf{J}}\cdot\overline{\mathbf{B}}\rangle + \langle \mathbf{j}\cdot\mathbf{b}\rangle = 0 \quad \text{(in the steady state)}. \tag{8}$$

If the field is fully helical, we have $\mu_0\langle \overline{\mathbf{J}}\cdot\overline{\mathbf{B}}\rangle = \mp k_1\langle \overline{\mathbf{B}}^2\rangle$ and $\mu_0\langle \mathbf{j}\cdot\mathbf{b}\rangle = \pm k_{\rm f}\langle \mathbf{b}^2\rangle$, where the upper (lower) sign applies to the case where the small scale helicity at the forcing scale is positive (negative). We then have from (8)

$$\langle \overline{\mathbf{B}}^2\rangle = (k_{\rm f}/k_1)\,\langle \mathbf{b}^2\rangle. \tag{9}$$

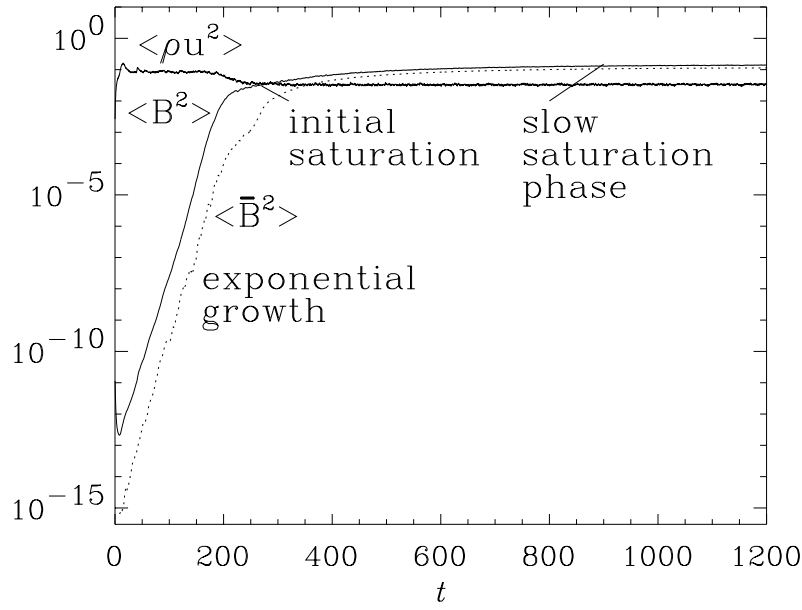

Fig. 3. The three stages of the magnetic field growth: exponential growth until initial saturation (when $\langle \mathbf{B}^2 \rangle / \mu_0 = \langle \rho \mathbf{u}^2 \rangle$), followed by a (resistively) slow saturation phase. In this plot we have used $\mu_0 = 1$. The energy of the large scale magnetic field, $\langle \overline{\mathbf{B}}^2 \rangle$, is shown for comparison. The data are from Run 3 of [19].

To a good approximation, $\langle \mathbf{b}^2 \rangle^{1/2}$ will be close to the equipartition field strength, $B_{\rm eq}$, so

$$\langle \overline{\mathbf{B}}^2 \rangle / B_{\rm eq}^2 \approx k_{\rm f}/k_1 > 1. \tag{10}$$

This means that the energy of the large scale field must, in the final state, be in super-equipartition by a factor approximately equal to the scale separation. We recall that this applies to the case of periodic boundaries. For closed (e.g. perfectly conducting) boundaries, $\langle \overline{\mathbf{B}}^2 \rangle$ can be even larger than $k_{\rm f}/k_1$ times the equipartition value [23]. This is because the large scale field is no longer fully helical, while the small scale field still is. In the presence of *open* boundaries, on the other hand, the large scale field will generally be smaller than suggested by (10), unless the boundaries transmit preferentially small scale fields (Sect. 4).

3.4 Sensitivity to Using Hyperdiffusivity

The above statements can readily be generalized to the case where the usual magnetic diffusion operator, $\eta \nabla^2$, is replaced by hyperdiffusion, $(-1)^{n-1} \eta_n \nabla^{2n}$ with $n = 2$. This implies that the diffusion has now become more strongly

wavenumber dependent; from ηk^2 to $\eta_2 k^4$. If the diffusion is the same at small scales, then the diffusion at large scales must be significantly smaller in the hyperdiffusive runs. This leads to a dramatic *increase* of the resistive saturation time. At the same time the final saturation field strength is no longer given by (10). The rate of magnetic helicity dissipation is now no longer proportional to k, but to k^3. Therefore the final saturation field strength is given by

$$\langle \overline{\mathbf{B}}^2 \rangle / B_{\rm eq}^2 \approx (k_{\rm f}/k_1)^3 \gg 1. \tag{11}$$

This result was confirmed also numerically [44]. Again, this applies to periodic boundaries. Hyperdiffusion has been used in the past in connection with open boundaries [6,45], but it is not clear how serious the possible artifacts from hyperdiffusion would be in such cases with open boundaries.

3.5 The Magnetic Helicity Constraint

The case of periodic boundaries is particularly useful as a benchmark to all dynamos exhibiting large scale dynamo action due to the helicity effect. Here we discuss the functional form $\overline{\mathbf{B}}^2(t)$ for the late saturation phase.

Equation (8) allows us not only to determine the final saturation strength, but also the approximate time evolution near saturation. As before, we make the assumption of fully helical fields. However, given that prior to saturation $|\langle \mathbf{j} \cdot \mathbf{b} \rangle| \approx |\langle \overline{\mathbf{J}} \cdot \overline{\mathbf{B}} \rangle|$, we must have $|\langle \mathbf{a} \cdot \mathbf{b} \rangle| \ll |\langle \overline{\mathbf{A}} \cdot \overline{\mathbf{B}} \rangle|$, so we can set

$$\langle \mathbf{A} \cdot \mathbf{B} \rangle \approx \langle \overline{\mathbf{A}} \cdot \overline{\mathbf{B}} \rangle = \mp k_1^{-1} \langle \overline{\mathbf{B}}^2 \rangle, \tag{12}$$

where the upper (lower) sign refers to positive (negative) small scale (kinetic and magnetic) helicity. Inserting this into (7) we have

$$k_1^{-1} \frac{\mathrm{d}}{\mathrm{d}t} \langle \overline{\mathbf{B}}^2 \rangle = -2\eta k_1 \langle \overline{\mathbf{B}}^2 \rangle + 2\eta k_{\rm f} \langle \mathbf{b}^2 \rangle. \tag{13}$$

The small scale field saturates first, so (13) can then be integrated to get the *subsequent* evolution of $\langle \overline{\mathbf{B}}^2 \rangle$ toward full saturation [19]

$$\langle \overline{\mathbf{B}}^2 \rangle = \frac{k_{\rm f}}{k_1} \langle \mathbf{b}^2 \rangle \left[1 - e^{-2\eta k_1^2 (t - t_{\rm sat})} \right] \quad (\text{for } t > t_{\rm sat}), \tag{14}$$

where $t_{\rm sat}$ is the time when the small scale field has reached saturation. Equation (14) is what we usually mean by the *magnetic helicity constraint*.

3.6 Inverse Cascade versus α-Effect

The process outlined above can be interpreted in two different ways: inverse cascade of magnetic helicity and/or α-effect. The two are similar in that they tend to produce magnetic energy at scales larger than the energy-carrying scale of the turbulence. As can be seen from Figs 1 and 2, the present simulations

support the notion of *nonlocal* inverse transfer [19]. This is not really an inverse cascade in the usual sense, because there is no sustained flux of energy through wavenumber space as in the direct Kolmogorov cascade. Instead, there is just a bump traveling to smaller k in wavenumber space. In that respect, the present simulations seem to differ from the Eddy Damped Quasi-Normal Markovian (EDQNM) closure approximation [46].

The other interpretation is in terms of the α-effect. We recall that there is a wavenumber $k_{\max}$ where the growth of the large scale field is largest; see (2). For reasonable estimates, $k_{\max}$ coincides with the position of the secondary bump in the spectrum ([19], Sect. 3.5). This can be taken as evidence in favor of the α-effect. In the nonlinear regime, the secondary bump travels to the left in the spectrum (i.e. toward smaller k). In the EDQNM picture this has to do with the equilibration of kinetic and current helicities at progressively smaller wavenumbers, which then saturates further growth at that wavenumber, but permits further growth at smaller wavenumbers until equilibration occurs. Another interpretation is simply that if α is quenched to a smaller value, $k_{\max} = \alpha/(2\eta_{\rm T})$ peaks at smaller wavenumbers where the growth has not yet saturated, until equilibration is attained also at that scale.

3.7 Implications

The growth of the large scale magnetic field can be interpreted as being due to the α-effect. Consequently, a slow-down in the final saturation phase must have to do with a suppression of α. According to closure models [46], the α-effect is really the residual between two competing effects: a kinematic helicity effect (which itself decreases somewhat for strong magnetic fields), and a current helicity effect of opposite sign. In Sect. 7 we shall use this phenomenology in a mean-field model where an explicitly time-dependent equation for the current helicity is solved. It turns out that in this model the late saturation phase is resistively limited–just like in the simulations.

It is somewhat worrisome that in the nonlinear regime the value of α depends on the microscopic magnetic diffusivity, which is very small in most astrophysical situations. One might therefore be concerned that in astrophysical dynamos the saturation would be unacceptably slow. In order to say more about α and also the turbulent magnetic diffusivity $\eta_{\rm t}$, we need to determine how α and $\eta_{\rm t}$ depend on $\mathbf{B}$. This can either be done directly [47], which is difficult and the results are noisy, or we can compare with models that incorporate the effects of α and $\eta_{\rm t}$ quenching. Before we do this (Sects 6 and 7), we first want to assess the effects of boundaries.

4 Open Boundaries: Good or Bad?

Boundaries generally lead to a loss of magnetic field both on small and large scales. Losses at large scale tend to lower the saturation field strength of the mean field. Losses of small scale fields can, at least in principle, enhance the

large scale field [21,22]. This has been demonstrated in an idealized numerical experiment [23], where the magnetic field at the forcing wavenumber and beyond had been removed in regular time intervals; see Fig. 4. We discuss this now in more detail.

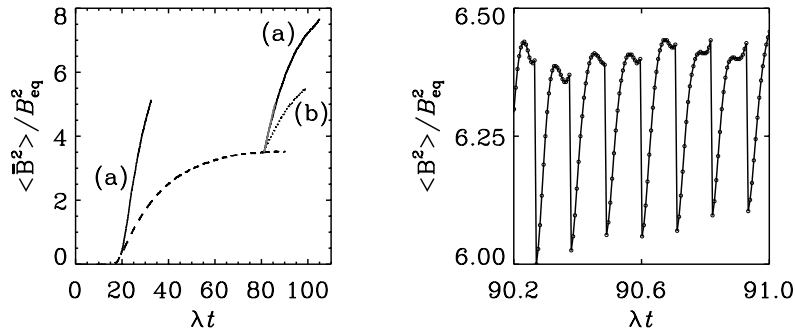

Fig. 4. The effect of removing small scale magnetic energy in regular time intervals Δt on the evolution of the large scale field (solid lines). The dashed line gives the evolution of $\langle \overline{\mathbf{B}}^2 \rangle$ for Run 3 of [19] (where no such energy removal was included) in units of $B_{\rm eq}^2 = \mu_0 \rho_0 \langle \mathbf{u}^2 \rangle$. The two solid lines show the evolution of $\langle \overline{\mathbf{B}}^2 \rangle$ after restarting the simulation from Run 3 of [19] at $\lambda t = 20$ and $\lambda t = 80$. Time is scaled with the kinematic growth rate λ. The curves labeled (a) give the result for $\Delta t = 0.12\lambda^{-1}$ and those labeled (b) for $\Delta t = 0.4\lambda^{-1}$. The second panel shows, for a short time interval, the sudden drop and subsequent recovery of the total (small and large scale) magnetic energy in regular time intervals. (Adapted from [23].)

4.1 Enhancement through Losses at Small Scales

The enhancement of large scale field by losses at small scales may seem somewhat mysterious. One way to interpret this result is by saying that the slow growth occurred because the energy of the small scale magnetic field has already reached the level of the kinetic energy, and only the large scale field has not yet saturated. After small scale magnetic fields have been removed, the field is for a short time interval in sub-equipartition at small scales and so the overall field (both at small and large scales) can then grow further during the short time interval during which the small scale field has not yet fully recovered to the equipartition value. The effect of a single such event is small, but many such events can produce a significant effect. This is exactly what is seen. Another way of interpreting this result is in terms of mean-field theory where the α-effect is saturated by a cancelation of kinetic and current helicities. If small scale magnetic fields are removed, the residual α-effect can be larger for some time interval, which then allows the field to grow further. In the following we illuminate this

result further by considering a modified magnetic helicity constraint for the case of open boundaries.

4.2 The Modified Magnetic Helicity Constraint

In Sect. 3.5 we have discussed an equation for the evolution of the magnetic energy of the large scale field at late times. Here we have assumed that there is no loss of magnetic energy and magnetic helicity through the boundaries. This equation has been generalized to account for losses of *large scale* magnetic helicity [20,23]. The idea is that there will be a magnetic helicity flux that is proportional to the gradient of the large scale magnetic helicity density (in a fixed gauge), and hence to the gradient of the magnetic energy density. This gives rise to an extra diffusion term, and hence to a renormalized, *effective* magnetic diffusivity, $\eta_{\rm eff}^{(1)}$, i.e. the term $2\eta k_1\langle\overline{\mathbf{B}}^2\rangle$ has to be replaced by $2\eta_{\rm eff}^{(1)}k_1\langle\overline{\mathbf{B}}^2\rangle$. Therefore, (13) takes the form [23]

$$k_1^{-1}\frac{\mathrm{d}}{\mathrm{d}t}\langle\overline{\mathbf{B}}^2\rangle = -2\eta_{\rm eff}^{(1)}k_1\langle\overline{\mathbf{B}}^2\rangle + 2\eta k_{\rm f}\langle\mathbf{b}^2\rangle, \tag{15}$$

which has the solution

$$\langle\overline{\mathbf{B}}^2\rangle = \frac{\eta k_{\rm f}}{\eta_{\rm eff}^{(1)}k_1}\langle\mathbf{b}^2\rangle\left[1-e^{-2\eta_{\rm eff}^{(1)}k_1^2(t-t_{\rm sat})}\right] \quad (\text{for } t>t_{\rm sat}), \tag{16}$$

Note that the saturation amplitude is decreased by a factor $\eta/\eta_{\rm eff}^{(1)}$ compared with (14), but at the same time the e-folding time has decreased to $(2\eta_{\rm eff}^{(1)}k_1^2)^{-1}$. We return to this behavior in the next subsection.

When the losses through the surface occur preferentially at small scales, an effective diffusivity would instead affect the small scale helicity flux. Therefore, (14) takes then the form

$$k_1^{-1}\frac{\mathrm{d}}{\mathrm{d}t}\langle\overline{\mathbf{B}}^2\rangle = -2\eta k_1\langle\overline{\mathbf{B}}^2\rangle + 2\eta_{\rm eff}^{(\rm f)}k_{\rm f}\langle\mathbf{b}^2\rangle, \tag{17}$$

which has the solution

$$\langle\overline{\mathbf{B}}^2\rangle = \frac{\eta_{\rm eff}^{(\rm f)}k_{\rm f}}{\eta k_1}\langle\mathbf{b}^2\rangle\left[1-e^{-2\eta k_1^2(t-t_{\rm sat})}\right] \quad (\text{for } t>t_{\rm sat}), \tag{18}$$

Note that the saturation amplitude is now increased by a factor $\eta_{\rm eff}^{(\rm f)}/\eta$ compared with (14), but the e-folding time, $(2\eta k_1^2)^{-1}$, is still resistively limited. This is in good agreement with what is seen in the simulations; see Fig. 4. In reality, there will be both small and large-scale losses, so the large scale magnetic energy is expected to evolve according to

$$\langle\overline{\mathbf{B}}^2\rangle = \frac{\eta_{\rm eff}^{(\rm f)}k_{\rm f}}{\eta_{\rm eff}^{(1)}k_1}\langle\mathbf{b}^2\rangle\left[1-e^{-2\eta_{\rm eff}^{(1)}k_1^2(t-t_{\rm sat})}\right] \quad (\text{for } t>t_{\rm sat}). \tag{19}$$

This equation allows time scales and saturation amplitudes that are not resistively limited.

4.3 Simulations with Open Boundaries

So far, simulations have not yet shown that the losses of small-scale magnetic fields are actually stronger than those of large-scale fields. Simulations with a vertical field (pseudo-vacuum) boundary condition have shown that most of the magnetic energy is lost at small scales [20]. The way this affects the slow resistively limited saturation process discussed earlier is by simply cutting off the saturation process at an earlier time, without changing the approximately linear slope past the initial saturation; cf. (16). In Fig. 5 we demonstrate a very similar behavior in another system which is actually periodic, but the helicity of the forcing is modulated in the z-direction such that the sign of the kinetic helicity changes in the middle. One can therefore view this system as two subsystems with a boundary in between. This boundary would correspond to the equator in a star or the midplane in a disc.

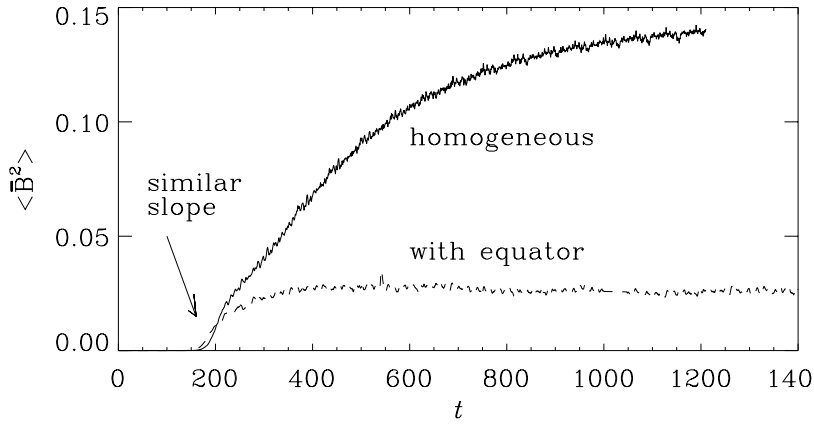

Fig. 5. Evolution of the magnetic energy for a run with homogeneous forcing function (solid line) and a forcing function whose helicity varies sinusoidally throughout the domain (dotted line) simulating the effects of equators at the two nodes of the sinusoidal helicity profile.

A somewhat surprising property of the models with variation of helicity in the z-direction is the fact that the mean field varies mostly in the x-direction, i.e. it follows the variation of the background model only weakly; see Fig. 6. Therefore, the mean field must be allowed to be two-dimensional, i.e.

$$\overline{\mathbf{B}}(x,z,t) = \int \mathbf{B} \mathrm{d}y \,\Big/ \int \mathrm{d}y. \tag{20}$$

Similar behavior was also found in simulations with boundaries, especially when the aspect ratio was large [23]. In the present context we were able to confirm, using a two-dimensional mean field dynamo in periodic geometry, that for $\alpha \propto \sin k_1 z$ the most easily excited mode varies indeed both in x and z; see Fig. 7.

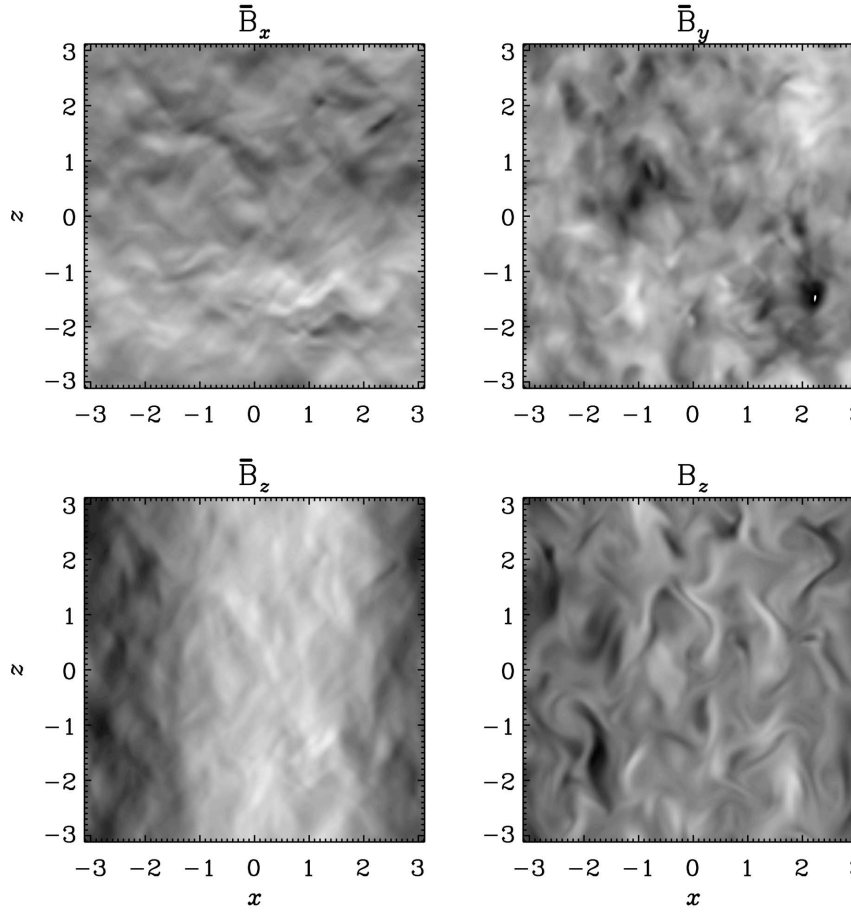

Fig. 6. Images of the three components of the mean field (averaged over the y-direction) for a run with sinusoidally varying helicity in the z-direction. Note that the most pronounced component of the mean field is actually $\overline{B}_z(x)$. The large-scale field is also visible in a y-slice of $\overline{B}_z$ (last panel).

In the simulations presented so far, boundaries merely tend to *reduce* the final saturation field strength. Thus, the idea to enhance the large scale field by small scale losses is not currently supported by simulations. It is quite possible, however, that this is simply a consequence of too simple a representation of the physical boundary. In the sun, coronal mass ejections are quite vigorous events that are known to shed large amounts of helical magnetic fields [28,29,30,31]. This kind of physics is not at all represented by adopting vacuum or pseudo-vacuum (vertical field) boundary conditions, as was done in [23].

We may then conclude that in simulations of large scale dynamos with relatively simple boundary conditions, open boundaries tend to be more important for large scale fields than for small scale fields. Although more realistic bound-

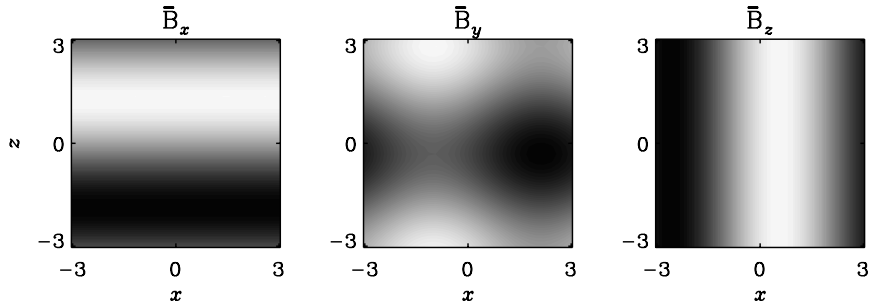

Fig. 7. Images of the three components of the mean field for an α^2 dynamo with sinusoidally varying α-effect in the z-direction. The $\overline{B}_x$ and $\overline{B}_z$ components resemble those in the direct simulation shown in Fig. 6.

ary conditions still need to be considered, it is useful to study more carefully whether, on observational grounds, a resistively limited dynamo can indeed be clearly excluded.

5 How Long Is Long? – Or What the Skin Depth Has to Do with the Solar Cycle

In this section we want to estimate the amount of magnetic helicity that is to be expected for a model of the solar dynamo. We also need to know which fraction of the magnetic field takes part in the 11-year cycle. Following an approach similar to that of Berger [48], we can bound the rate of change of magnetic helicity in terms of the rate of Joule dissipation, $Q_{\rm Joule}$, and magnetic energy, M. For an oscillatory dynamo, all three variables, H, M, and $Q_{\rm Joule}$ vary in an oscillatory fashion with a cycle frequency ω of magnetic energy (corresponding to 11 years for the sun – not 22 years), so we estimate $|{\rm d}H/{\rm d}t| \lesssim \omega|H|$ and $Q_{\rm Joule} \lesssim \omega M$, which leads to the inequality [23,44]

$$|H|/(2\mu_0 M) \leq \ell_{\rm skin}, \tag{21}$$

where $\ell_{\rm skin} = (2\eta/\omega)^{1/2}$ is the skin depth, here associated with the oscillation frequency ω. Thus, the maximum magnetic helicity that can be generated and dissipated during one cycle is characterized by the length scale $|H|/(2\mu_0 M)$, which has to be less than the skin depth $\ell_{\rm skin}$.

For η we have to use the Spitzer resistivity which is proportional to $T^{-3/2}$ (T is temperature), so η varies between $10^4\,{\rm cm}^2/{\rm s}$ at the base of the convection zone to about $10^7\,{\rm cm}^2/\,{\rm s}$ near the surface layers and decreases again in the solar atmosphere. Using $\omega = 2\pi/(11\,{\rm yr}) = 2\times10^{-8}\,{\rm s}^{-1}$ for the relevant frequency at which H and M vary we have $\ell_{\rm skin} \approx 10\,{\rm km}$ at the bottom of the convection zone and $\ell_{\rm skin} \approx 300\,{\rm km}$ at the top.

This needs to be compared with the value $|H|/(2\mu_0 M)$ obtained from dynamo models. Although mean-field theory has been around for several decades,

the helicity aspect has only recently attracted significant attention. In the proceedings of a meeting devoted specifically to this topic [49], magnetic helicity was discussed extensively also in the context of mean-field theory. However, the precise amount of magnetic helicity relative to the magnetic energy, and the possibility of helicity reversals at some length scale were not addressed at the time, although the evolution of the current helicity has already been investigated in the context of a mean field model [50].

For a sphere (or a half-sphere) with open boundary conditions and volume V (for example the northern hemisphere), one has to use the gauge-invariant relative magnetic helicity of Berger & Field [43],

$$H = \int_V (\mathbf{A} + \mathbf{A}_\mathrm{P}) \cdot (\mathbf{B} - \mathbf{B}_\mathrm{P}) \, \mathrm{d}V, \tag{22}$$

where $\mathbf{B}_\mathrm{P} = \boldsymbol{\nabla} \times \mathbf{A}_\mathrm{P}$ is a potential field used as reference field that has on the boundaries the same normal component as $\mathbf{B}$. Any additional gradient terms, $\boldsymbol{\nabla}\phi$, in $\mathbf{A}$ or $\mathbf{A}_\mathrm{P}$ yield only a surface term,

$$\int_{\partial V} \phi(\mathbf{B} - \mathbf{B}_\mathrm{P}) \cdot \mathrm{d}\mathbf{S}, \tag{23}$$

which vanishes because $\mathbf{B}_\mathrm{P} \cdot \boldsymbol{n} = \mathbf{B} \cdot \boldsymbol{n}$. When applied to an axisymmetric mean field, which can be written as $\overline{\mathbf{B}} = b\hat{\boldsymbol{\phi}} + \boldsymbol{\nabla} \times a\hat{\boldsymbol{\phi}}$, it turns out that the relative magnetic helicity integral is simply [23]

$$H = 2 \int_V ab \, \mathrm{d}V. \tag{24}$$

In order to see how the condition (21) is met by mean-field models, we have calculated a typical $\alpha\Omega$ model relevant to the sun and evaluated (24) over the volume of the northern hemisphere [23].

We recall that in the Babcock-Leighton approach it is mainly the latitudinal differential rotation that enters. We also note that, although the latitudinal migration could be explained by radial differential rotation, meridional circulation is in principle able to drive meridional migration even when the sense of radial differential rotation would otherwise be wrong for driving meridional migration [15,51,52]. Therefore, we have considered the simple models in spherical geometry. The results of such a model show that [23], once $B_\mathrm{pole}/B_\mathrm{belt}$ is in the range consistent with observations, $B_\mathrm{pole}/B_\mathrm{belt} = (1...3) \times 10^{-4}$, $H_\mathrm{N}/(2\mu_0 M_\mathrm{N} R)$ is around $(2-5) \times 10^{-4}$ for models with latitudinal shear. (Here, the subscript 'N' refers to the northern hemisphere.) This confirms the scaling

$$H_\mathrm{N}/(2\mu_0 M_\mathrm{N} R) = \mathcal{O}(B_\mathrm{pol}/B_\mathrm{tor}) \gtrsim B_\mathrm{pole}/B_\mathrm{belt}. \tag{25}$$

Given that $R = 700\,\mathrm{Mm}$ this means that $H_\mathrm{N}/(2\mu_0 M_\mathrm{N}) \approx 70...200\,\mathrm{km}$, which would be comparable with the value of ℓ_skin near the upper parts of the solar convection zone, or for models with only latitudinal shear.

The surprising conclusion is that the amount of mean field helicity that needs to be generated in order to explain the large scale solar magnetic fields is so small,

that it may be plausible that microscopic magnetic diffusion could still play a role in the solar dynamo. In other words, open boundary effects may well be important for understanding the time scale of the dynamo, but the effect does not need to be extremely strong.

6 Connection with α-Quenching

Nonlinear helical dynamos in a periodic domain are particularly simple. They provide therefore an ideal benchmark for models of α-quenching. Before applying models to more complicated situations, they should pass the test of predicting the right behavior in the simple case of an α^2-dynamo. By "right behavior" we mean that the large-scale magnetic field saturates as seen in (14). While this is already a relatively stringent test that allows us to eliminate some earlier models (see Sect. 6.2), we point out that the complete time evolution (including the early kinematic exponential growth phase) can only be described correctly by an explicitly time-dependent evolution equation for α that ensures that the magnetic helicity equation is obeyed exactly at all times.

6.1 The Lorentzian Quenching Formula

We first assume that both α-effect and the turbulent magnetic diffusivity, $\eta_{\rm t}$, are being affected by the magnetic field. In the first class of models we assume

$$\alpha = \alpha_0\, q(\overline{\mathbf{B}}), \quad \eta_{\rm t} = \eta_{\rm t0}\, q(\overline{\mathbf{B}}), \tag{26}$$

i.e. we postulate the existence of an algebraic quenching formula for both α and $\eta_{\rm t}$. The models that work best are those with a lorentzian quenching formula,

$$q(\overline{\mathbf{B}}) = \frac{1}{1 + a\overline{\mathbf{B}}^2/B_{\rm eq}^2} \quad \text{(lorentzian formula)}, \tag{27}$$

where a is a dimensionless coefficient and $B_{\rm eq}$ is the equipartition field strength with $B_{\rm eq}^2/\mu_0 = \langle \rho \mathbf{u}^2 \rangle$.

For an α^2-dynamo in a periodic box, the coefficient a can be readily determined. This is because here we actually know the final saturation field strength; see (10). In a mean-field model, on the other hand, where quenching is the only nonlinearity, the saturation field strength is proportional to $a^{-1/2}$. In order to work out the coefficients, we consider the α^2 mean-field equation for a Beltrami field with wavenumber k_1. The evolution of the mean-squared field strength is then governed by [19]

$$\tfrac{1}{2}\frac{\rm d}{{\rm d}t}\ln\langle\overline{\mathbf{B}}^2\rangle = \frac{\alpha_0 k_1 - \eta_{\rm t0} k_1^2}{1 + a\langle\overline{\mathbf{B}}^2\rangle/B_{\rm eq}^2} - \eta k_1^2. \tag{28}$$

In the steady state, the right hand side of (28) has to vanish, so

$$\frac{\alpha_0 k_1 - \eta_{\rm t0} k_1^2}{1 + a\langle\overline{\mathbf{B}}^2\rangle/B_{\rm eq}^2} - \eta k_1^2 = 0, \tag{29}$$

or, using (10),

$$a = \frac{\alpha_0 - \eta_{t0} k_1}{\eta k_f} \equiv \frac{\lambda}{\eta k_f k_1} \tag{30}$$

(see [19]). The main point here is that the parameter a scales with the magnetic Reynolds number, so it is very large under astrophysical circumstances. Moreover, if the growth rate λ scales with the inverse turnover time on the forcing scale, then the k_f in the denominator cancels and a is proportional to the magnetic Reynolds number [53,54,55]. This is also consistent with the analysis of [56].

A consequence of the large value of a is a very slow saturation phase and not necessarily a very low saturation level, as is usually believed [54]. That the saturation phase is slow can be seen, for example, by considering the magnitude of the right hand side of (28) near saturation, so we put

$$\langle \overline{\mathbf{B}}^2 \rangle / B_{eq}^2 = (1 - \epsilon) k_f / k_1, \tag{31}$$

which means that we are a fraction ϵ away from full equipartition. We then have

$$\text{rhs of (28)} = \frac{\alpha_0 k_1 - \eta_{t0} k_1^2}{1 + \frac{\alpha_0 k_1 - \eta_{t0} k_1^2}{\eta k_f} (1 - \epsilon) \frac{k_f}{k_1}} - \eta k_1^2. \tag{32}$$

Since the field is already strong, the '1+' in the denominator may be neglected, so we obtain

$$\text{rhs of (28)} = \left[\frac{\alpha_0 k_1 - \eta_{t0} k_1^2}{(\alpha_0 k_1 - \eta_{t0} k_1^2)(1 - \epsilon)} - 1 \right] \eta k_1^2 = \frac{\epsilon}{1 - \epsilon} \eta k_1^2 \approx \epsilon \eta k_1^2. \tag{33}$$

The rhs of (28) can be regarded as a local growth rate if the field was unchanged. The extrapolated saturation time would therefore be $(\epsilon \eta k_1^2)^{-1}$, which is more than a resistive time!

6.2 Other Quenching Formulae

By contrast, consider a quenching of the form

$$q(\overline{\mathbf{B}}) = 1 - a \overline{\mathbf{B}}^2 / B_{eq}^2 \quad \text{(quadratic formula)}. \tag{34}$$

To match the right saturation field strength we have to have

$$(\alpha_0 k_1 - \eta_{t0} k_1^2)(1 - a k_f / k_1) - \eta k_1^2 = 0. \tag{35}$$

This gives

$$a = \frac{\alpha_0 k_1 - \eta_{T0} k_1^2}{\alpha_0 k_1 - \eta_{t0} k_1^2} \frac{k_1}{k_f} \to \frac{k_1}{k_f} \quad \text{for small } \eta. \tag{36}$$

Again, we calculate the instantaneous growth rate for a field that was close to final saturation, i.e. we put $\langle \overline{\mathbf{B}}^2 \rangle / B_{eq}^2 = (1 - \epsilon) k_f / k_1$. This gives

$$\text{rhs of (28)} = (\alpha_0 k_1 - \eta_{t0} k_1^2) \left[1 - \frac{\alpha_0 k_1 - \eta_{T0} k_1^2}{\alpha_0 k_1 - \eta_{t0} k_1^2} (1 - \epsilon) \right] - \eta k_1^2 \tag{37}$$

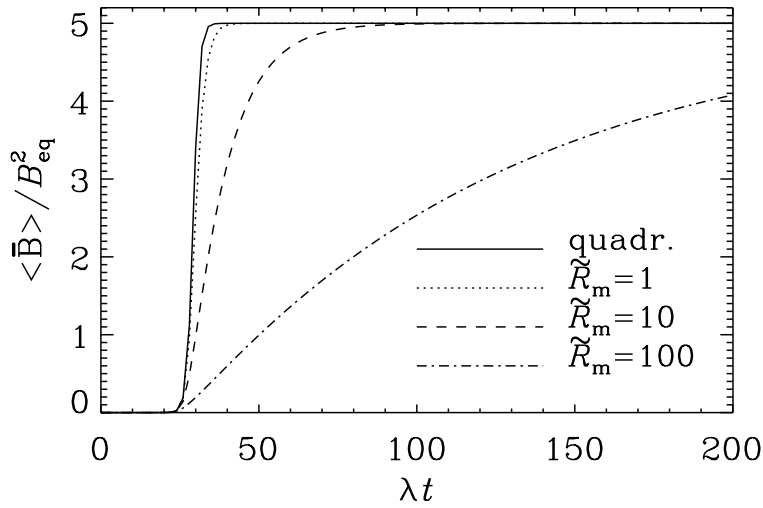

Fig. 8. Saturation behavior for the quadratic quenching formula (solid line) compared with different lorentzian quenching formulae with different values of $\tilde{R}_{\rm m} \equiv \lambda/(\eta k_1^2)$ (broken lines). Note the slow saturation behavior, consistent with (14). The results for the quadratic quenching formula are independent of the value of $\tilde{R}_{\rm m}$, which is therefore inconsistent with (14).

or, after some simplifications,

$$\text{rhs of (28)} = \epsilon(\alpha_0 k_1 - \eta_{\rm T0} k_1^2). \tag{38}$$

This means that it will only take a few dynamical time scales before the extrapolated field will reach final saturation, which is of course incompatible with the magnetic helicity constraint (14). Figure 8 shows the great discrepancy between these two quenching formulae. The quadratic quenching formula gives, for different values of $\tilde{R}_{\rm m} \equiv \lambda/(\eta k_1^2)$, always the same saturation behavior, while the lorentzian formula gives a more prolonged saturation phase as $\tilde{R}_{\rm m}$ is increased.

One may still be tempted to expect that there could be many other quenching formulae that might work as well. One clear counter example is shown in Fig. 9 where we compare the results from a cubic quenching formula with the magnetic helicity constraint in (14). For the cubic quenching we just used the very simple formula $q = 1/(1+\beta^3)$, where $\beta^2 = a\langle\overline{\mathbf{B}}^2\rangle/B_{\rm eq}^2$. The departure between cubic is not very strong, but clearly noticeable. We note that if we replaced $\eta \to \frac{3}{2}\eta$, the helicity constraint would actually fit, but of course η is an input parameter, so we cannot just adopt a different value in the analysis. We may therefore conclude that cubic quenching can be ruled out.

Finally, we consider a quenching formula that has the correct strong field asymptotics, $q \to \beta^{-2}$, and also the same weak field Taylor expansion as the

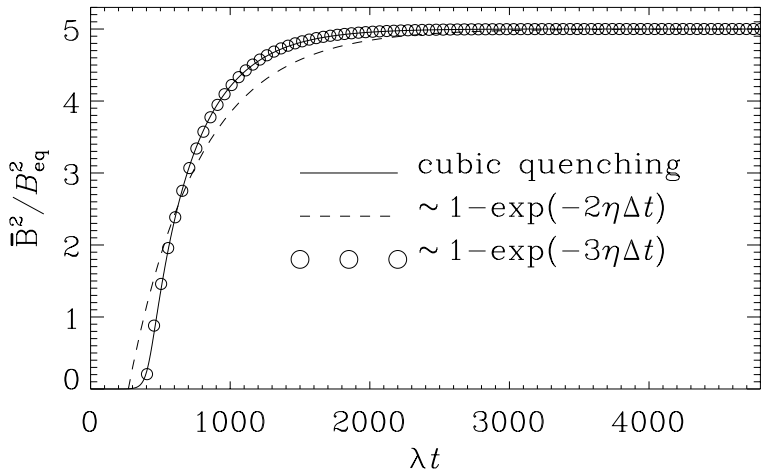

Fig. 9. Saturation behavior for cubic quenching (solid line) compared with the magnetic helicity constraint (dashed line). Note also that if we used the *wrong* microscopic diffusivity, $\eta \to \frac{3}{2}\eta$, the helicity constraint would actually fit.

lorentzian formula, $q \approx 1 + \beta^2$,

$$q(\overline{\mathbf{B}}) = \frac{1}{\beta^2}\left(1 - \frac{\tan^{-1}\sqrt{3\beta^2}}{\sqrt{3\beta^2}}\right), \quad \text{where} \;\; \beta^2 = a\langle\overline{\mathbf{B}}^2\rangle/B_{\mathrm{eq}}^2. \tag{39}$$

This expression entered in the quenching formula derived by Field, Blackman, & Cho [57]. In Fig. 10 we compare the saturation behavior for the atan formula with the lorentzian one. Clearly, the atan formula is much better than any of the other formulae considered in this subsection, but the lorentzian formula is still considerably closer to the magnetic helicity constraint than the atan formula.

6.3 Non-universality of the Lorentzian Quenching Formula

We may now be under the impression that the lorentzian formula is probably the correct quenching expression. While is does indeed provide a good description of what is going on in the simulations, we note that there are also a few problems. Firstly, when applied to other models where the field is in general no longer isotropic and force-free (e.g., if there is shear or if there are boundaries) the best fit value of a is no longer equal to the value calculated for the α^2-dynamo; see (30).

The other problem is rather an uncomfortable prediction from the quenching model with the lorentzian formula. Since both α and η_{t} are quenched by equal amounts, η_{t} will become comparable with η near full saturation. As a consequence, the cycle period of $\alpha\Omega$-dynamo models becomes comparable to the resistive time which is rather long. So, mean-field theory of the solar dynamo may face a very serious problem, unless open boundary effects (Sect. 4) play an

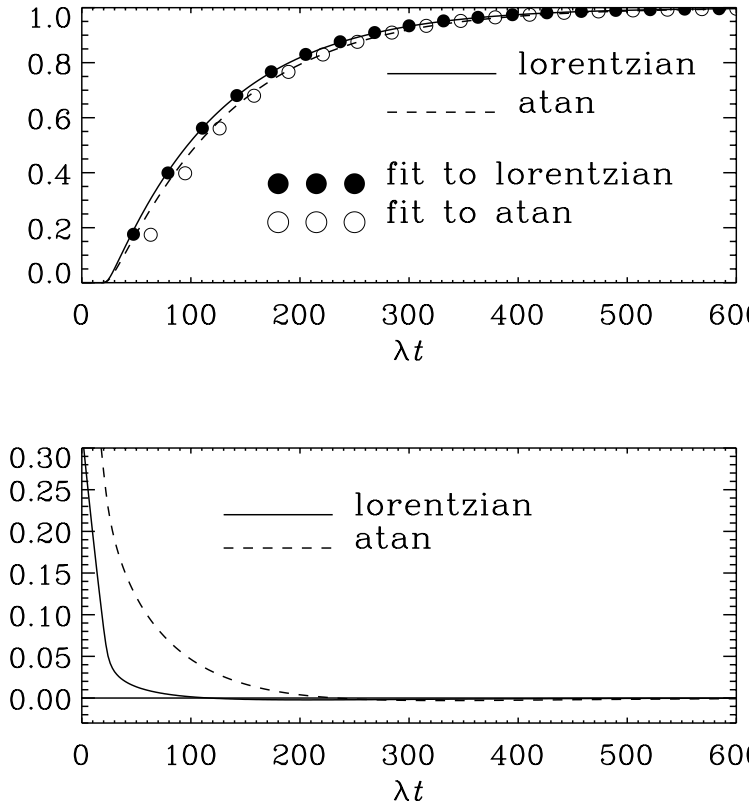

Fig. 10. Comparison of the saturation behavior for the lorentzian and atan formulae, together with the corresponding fits obtained from the helicity constraint.

important role. Simulations perhaps seem to point into this direction as well: the cycle period found in simulations with shear [58] was already rather long, and with a further reduction of the magnetic diffusivity by a factor of 2.5, the cycles disappeared altogether [23]. On the other hand, the absence of cycles could have been for other reasons, for example due to too restricted a geometry (with sinusoidal shear flow on a scale only 5 times larger than the energy carrying scale of the turbulence). Thus, these two simulations are perhaps not yet fully conclusive.

In the following we point out that there is yet another possibility that is at least equally well in agreement with our α^2-dynamo benchmark result and theoretically more theoretically more appealing because it satisfies the magnetic helicity equation exactly at all times.

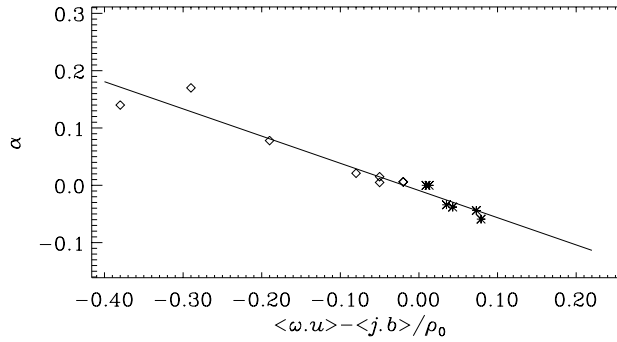

Fig. 11. Dependence of $\alpha = \overline{\mathcal{E}}_y/B_{0y}$ on the residual helicity, obtained by imposing a uniform magnetic field $\mathbf{B}_0 = (0,\ B_{0y},\ 0)$ and driving the turbulence either through the momentum equation (diamonds) or by an extra forcing term in the induction equation (asterisks).

7 Dynamical Quenching

A quenching formula that we have not yet discussed is the formula for the *residual* α-effect,

$$\alpha = \alpha_{\rm K} + \alpha_{\rm M} \quad \text{with} \quad \alpha_{\rm K} = -\frac{\tau}{3}\langle \boldsymbol{\omega}\cdot\mathbf{u}\rangle, \quad \alpha_{\rm M} = +\frac{\tau}{3\rho_0}\langle \mathbf{j}\cdot\mathbf{b}\rangle, \tag{40}$$

which is due to Pouquet, Frisch, and Léorat [46], and has frequently been used in connection with α-quenching [59,60,61,62]. The result that the α-effect is proportional to the *residual* helicity, $\langle \boldsymbol{\omega}\cdot\mathbf{u}\rangle - \langle \mathbf{j}\cdot\mathbf{b}\rangle/\rho_0$ has also been confirmed numerically [63] by imposing a uniform magnetic field and driving the turbulence either through the momentum equation (as is done in the rest of the paper) or through a forcing term in the induction equation; see Fig. 11.

The question now is how to use (40) in a mean field model, which only knows about the mean field, $\overline{\mathbf{B}}$. If we were to approximate $\langle \mathbf{j}\cdot\mathbf{b}\rangle$ in a direct manner by $\overline{\mathbf{B}}^2$, this would correspond to the quenching formula (34), which is clearly ruled out because it violates the magnetic helicity equation. On the other hand, we can explicitly make sure that the magnetic helicity equation (7) is obeyed. The contribution $\langle \overline{\mathbf{A}}\cdot\overline{\mathbf{B}}\rangle$ from the large scale fields to the magnetic helicity equation is automatically taken into account by the mean-field equation, so we only need to solve for the missing contribution from small scales, $\langle \mathbf{a}\cdot\mathbf{b}\rangle$, and the two equations for $\langle \overline{\mathbf{A}}\cdot\overline{\mathbf{B}}\rangle$ and $\langle \mathbf{a}\cdot\mathbf{b}\rangle$ must be fully coupled.

Another way of seeing this [64] is that, while $\langle \mathbf{A}\cdot\mathbf{B}\rangle$ stays close to zero on short enough time scales, any increase of the magnetic field by the α-effect leads to an increase of the large scale magnetic helicity, $\langle \overline{\mathbf{A}}\cdot\overline{\mathbf{B}}\rangle$. This can only be consistent with an almost unchanged $\langle \mathbf{A}\cdot\mathbf{B}\rangle$ if there is a simultaneous generation of small scale magnetic helicity, $\langle \mathbf{a}\cdot\mathbf{b}\rangle$, of opposite sign, so that

$$\langle \mathbf{A}\cdot\mathbf{B}\rangle = \langle \overline{\mathbf{A}}\cdot\overline{\mathbf{B}}\rangle + \langle \mathbf{a}\cdot\mathbf{b}\rangle \tag{41}$$

stays close to zero. The price to pay for this is that the small scale magnetic helicity can also produce an α-effect, $\alpha_{\rm M}=\frac{1}{3}\tau\langle\mathbf{j}\cdot\mathbf{b}\rangle/\rho_0$, but it has the opposite sign than $\alpha_{\rm K}$, so the residual α-effect becomes quenched. Mathematically, this quenching of α can be described by the magnetic helicity equation. The contribution of the large scale field to the magnetic helicity equation follows from the mean-field equation. The small scale contribution is exactly such that the sum of these two equations gives (7). Thus, we have a pair of two equations [64]

$$\frac{\mathrm{d}}{\mathrm{d}t}\langle\overline{\mathbf{A}}\cdot\overline{\mathbf{B}}\rangle=2\langle\overline{\boldsymbol{\mathcal{E}}}\cdot\overline{\mathbf{B}}\rangle-2\eta\mu_0\langle\overline{\mathbf{J}}\cdot\overline{\mathbf{B}}\rangle, \tag{42}$$

$$\frac{\mathrm{d}}{\mathrm{d}t}\langle\mathbf{a}\cdot\mathbf{b}\rangle=-2\langle\overline{\boldsymbol{\mathcal{E}}}\cdot\overline{\mathbf{B}}\rangle-2\eta\mu_0\langle\mathbf{j}\cdot\mathbf{b}\rangle. \tag{43}$$

where $\overline{\boldsymbol{\mathcal{E}}}=\overline{\mathbf{u}\times\mathbf{b}}$ is the mean turbulent electromotive force, for which we adopt the usual mean-field closure in terms of α-effect and turbulent magnetic diffusivity, i.e.

$$\overline{\boldsymbol{\mathcal{E}}}=\alpha\overline{\mathbf{B}}-\eta_{\rm t}\mu_0\overline{\mathbf{J}}. \tag{44}$$

Note that (42) follows directly from the usual mean-field dynamo equation (1). Making use of the relation $\mu_0\langle\mathbf{j}\cdot\mathbf{b}\rangle=k_{\rm f}^2\langle\mathbf{a}\cdot\mathbf{b}\rangle$ in (40), (43) becomes [56]

$$\frac{\mathrm{d}\alpha_{\rm M}}{\mathrm{d}t}=-2\eta k_{\rm f}^2\left(R_{\rm m}\frac{\langle\overline{\boldsymbol{\mathcal{E}}}\cdot\overline{\mathbf{B}}\rangle}{B_{\rm eq}^2}+\alpha_{\rm M}\right), \tag{45}$$

where $R_{\rm m}=\eta_{\rm t}/\eta$ is the appropriate definition in the present context.

An evolution equation for α was already proposed twenty years ago [65]; see also [66,67]. Nevertheless, dynamical quenching was usually ignored, although it has sometimes been used in mean-field models with the main motivation to promote and study chaotic behavior in stellar dynamos [68,69,70,71]. Kleeorin et al. [22] were the first to point out that the catastrophic quenching of Vainshtein & Cattaneo [54] is just a special case of dynamical quenching.

7.1 Adiabatic Approximation and Force-Free Degeneracy

Near the saturated state the explicit time derivative in (45), $\mathrm{d}\alpha_{\rm M}/\mathrm{d}t$, can be neglected and the value of $\alpha_{\rm M}$ adjusts 'adiabatically' as the field saturates. Thus, we have [56]

$$0=R_{\rm m}\frac{\langle\overline{\boldsymbol{\mathcal{E}}}\cdot\overline{\mathbf{B}}\rangle}{B_{\rm eq}^2}+\alpha_{\rm M}, \tag{46}$$

or, after substituting $\alpha_{\rm M}=\alpha-\alpha_{\rm K}$,

$$R_{\rm m}\left(\alpha\langle\overline{\mathbf{B}}^2\rangle-\eta_{\rm t}\langle\overline{\mathbf{J}}\cdot\overline{\mathbf{B}}\rangle\right)+(\alpha-\alpha_{\rm K})=0, \tag{47}$$

which yields

$$\alpha=\frac{\alpha_{\rm K}+R_{\rm m}\eta_{\rm t}\langle\overline{\mathbf{J}}\cdot\overline{\mathbf{B}}\rangle}{1+R_{\rm m}\langle\overline{\mathbf{B}}^2\rangle}. \tag{48}$$

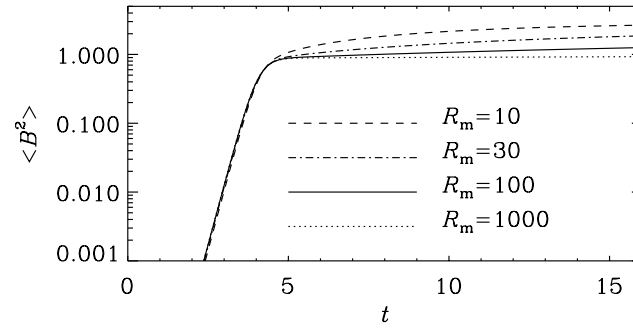

Fig. 12. The early saturation phase of the energy of the mean field in the dynamical quenching model for four different values of the magnetic Reynolds number.

This equation was already obtained by Gruzinov & Diamond [59,67]. The late saturation phase of α^2-dynamos is well described by (48). This is because near saturation time dependence is governed by the slow resistive adjustment in the mean field equation for the large-scale field, whilst the α equation is quickly adjusting to whatever the large-scale field is at any time.

The reason why the lorentzian quenching formula describes the resistively limited quenching behavior so well is because in the case of a nearly force free large scale magnetic field the lorentzian quenching formula and the adiabatic approximation become identical. Indeed, if the large-scale magnetic field is force-free, we have $\langle\overline{\mathbf{J}}\cdot\overline{\mathbf{B}}\rangle\overline{\mathbf{B}}=\langle\overline{\mathbf{B}}^2\rangle\overline{\mathbf{J}}$, which allows us to write the full electromotive force, $\overline{\boldsymbol{\mathcal{E}}}=\alpha\overline{\mathbf{B}}-\eta_{\rm t}\mu_0\overline{\mathbf{J}}$, in the form

$$\begin{aligned}\overline{\boldsymbol{\mathcal{E}}}&=\frac{\alpha_{\rm K}+R_{\rm m}\eta_{\rm t}\mu_0\langle\overline{\mathbf{J}}\cdot\overline{\mathbf{B}}\rangle/B_{\rm eq}^2}{1+R_{\rm m}\langle\overline{\mathbf{B}}^2\rangle/B_{\rm eq}^2}\,\overline{\mathbf{B}}-\eta_{\rm t0}\mu_0\overline{\mathbf{J}}\\&=\frac{\alpha_{\rm K}\overline{\mathbf{B}}}{1+R_{\rm m}\langle\overline{\mathbf{B}}^2\rangle/B_{\rm eq}^2}-\frac{\eta_{\rm t0}\mu_0\overline{\mathbf{J}}}{1+R_{\rm m}\langle\overline{\mathbf{B}}^2\rangle/B_{\rm eq}^2},\end{aligned}\tag{49}$$

which shows that in the force-free case the adiabatic approximation together with constant (unquenched) turbulent magnetic diffusivity becomes equal to the pair of expressions where both α and $\eta_{\rm t}$ are catastrophically quenched. This is called the force-free degeneracy [56]. This degeneracy is lifted in cases with shear or when the turbulence is no longer fully helical.

7.2 α^2-Dynamos

When applied to an α^2-dynamo model with dynamical quenching, the helicity constraint is well satisfied [56,64] and the difference between the solutions with dynamical and algebraic quenching turns out to be small if $R_{\rm m}$ is less than about 1000. The difference in the evolution of magnetic energy with dynamical

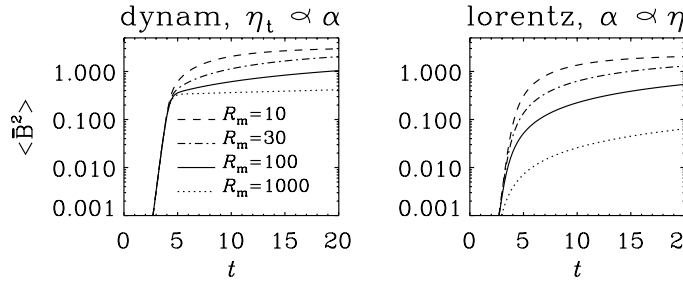

Fig. 13. The effects of assuming $\eta_t \propto \alpha$ in the dynamical and the lorentzian quenching models for four different values of the magnetic Reynolds number.

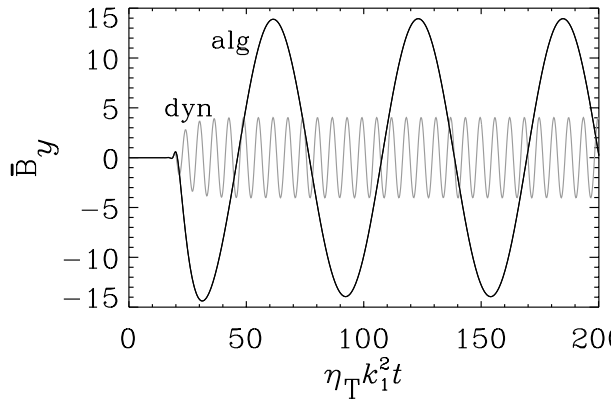

Fig. 14. Comparison of $\alpha\Omega$-dynamo models with algebraic (solid line) and dynamical quenching (grey line). $\Omega'/(\eta_T k_1^2) = 100$, $\alpha_K/(\eta_T k_1) = 0.1$, $R_m \equiv \eta_t/\eta = 10$.

quenching and with algebraic (or lorentzian) quenching, is only a few percent if the magnetic Reynolds number is small. The difference increases as the magnetic Reynolds number increases; see Fig. 13, where we plot the evolution of $\langle \overline{\mathbf{B}}^2 \rangle$ around the time when the kinematic exponential growth turns into the resistively limited saturation phase which was already described in Sect. 3.5. Conclusive agreement with simulations is at this point not possible, mostly because the magnetic Reynolds numbers are not large enough.

7.3 $\alpha\Omega$-Dynamos

When shear is included, toroidal field can be regenerated solely by the shear term. This is where dynamical and algebraic quenching lead to very different behaviors. With algebraic quenching, the reduction of η_t leads to resistively long cycle periods in the nonlinear regime. With dynamical quenching, η_t is

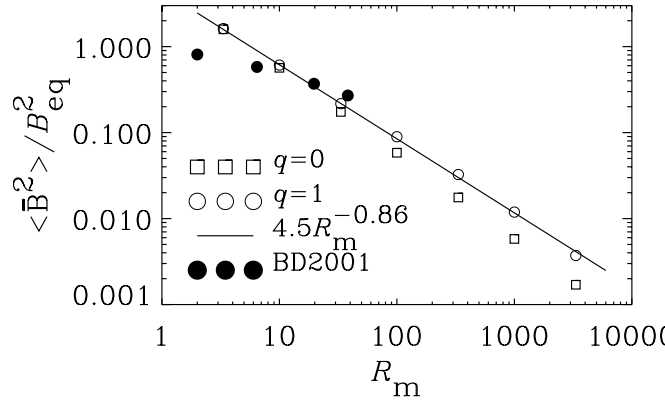

Fig. 15. Saturation energy versus $R_{\rm m}$ for α^2-dynamos with boundaries. Models with ($q = 1$) and without ($q = 0$) loss term are indicated by open circles and open squares, respectively. The line gives the fit $\langle\overline{\mathbf{B}}^2\rangle \sim R_{\rm m}^{-0.86}$. Simulations of [20] are shown as full circles.

constant and the cycle frequency remains of order unity; see Fig. 14. Here, $R_{\rm m}$ is only 10, but for larger values the final field amplitude and the cycle period are considerably enhanced.

7.4 Open Boundaries

Finally we consider a model with vertical field boundary conditions ($\overline{B}_x = \overline{B}_y = 0$ on $z = \pm\pi$) and solve the α^2-dynamo equation. The resulting mean-squared field strength is plotted in Fig. 15 versus $R_{\rm m}$. We find that $\langle\overline{\mathbf{B}}^2\rangle \sim R_{\rm m}^{-1}$, which is consistent with (16), but steeper than what was obtained in the simulations [20]. Kleeorin et al. [22,72] pointed out that in (45) there should be an additional loss term on the right hand side. By making this loss term suitably $R_{\rm m}$-dependent, one could in principle make the $R_{\rm m}$-dependence of $\langle\overline{\mathbf{B}}^2\rangle$ less steep, but some reduction is already obtained by allowing for a diffusion-like loss term of the form $q\eta_{\rm T}\nabla^2\alpha_{\rm M}$ on the right hand side; see the open circles in Fig. 15. The parameter q is used to regulate the efficiency of this loss. The simulations of [20] are shown as full circles.

7.5 Generalization to Nonuniform $\boldsymbol{\alpha}$

In all astrophysical bodies there are opposite signs of kinetic helicity, $\langle\boldsymbol{\omega}\cdot\mathbf{u}\rangle$, in the northern and southern hemispheres. In the approach of Kleeorin and collaborators [65,66,67] the dynamical α-quenching framework was always used as a theory for nonuniform α, which does not seem to be well justified. Most importantly, the connection between $\langle\mathbf{j}\cdot\mathbf{b}\rangle$ (in the expression for $\alpha_{\rm M}$) and $\langle\mathbf{a}\cdot\mathbf{b}\rangle$

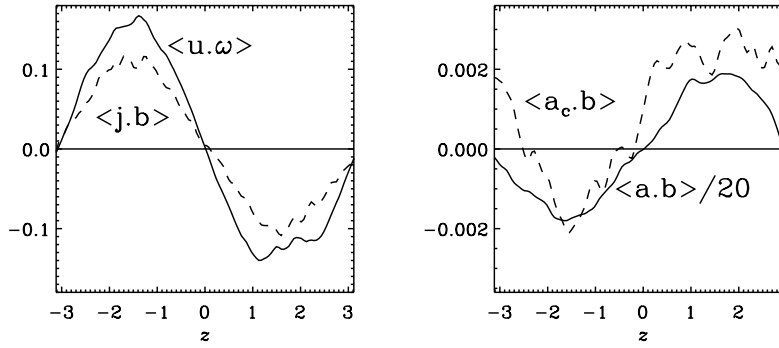

Fig. 16. Comparison of the horizontally averaged kinetic and current helicity densities, $\langle \boldsymbol{\omega} \cdot \mathbf{u} \rangle$ and $\langle \mathbf{j} \cdot \mathbf{b} \rangle$, respectively (left hand panel), and the horizontally averaged magnetic helicity densities in the $\phi = 0$ gauge $\langle \mathbf{a} \cdot \mathbf{b} \rangle$ and the Coulomb gauge $\langle \mathbf{a}_c \cdot \mathbf{b} \rangle$.

is no longer straightforward when the angular brackets denote ensemble averages (which are not really of practical interest) or averages over one or two periodic coordinate directions. Indeed, $\langle \mathbf{a} \cdot \mathbf{b} \rangle$ is no longer gauge-invariant, so one has to fix the gauge. The Coulomb gauge is the most common one, but one should realize that going to another gauge can make a major difference. In Fig. 16 we show the magnetic helicity in the $\phi = 0$ and the Coulomb gauges, $\langle \mathbf{a} \cdot \mathbf{b} \rangle$ and $\langle \mathbf{a}_c \cdot \mathbf{b} \rangle$, respectively (see Sect. 3). Note that the Coulomb gauged magnetic helicity is about twenty times smaller than that in the $\phi = 0$ gauge. More importantly, the magnetic helicity is *not* a positive multiple of the current helicity, $\langle \mathbf{j} \cdot \mathbf{b} \rangle$. (We recall that for homogeneous turbulence, $\langle \mathbf{j} \cdot \mathbf{b} \rangle = k_f^2 \langle \mathbf{a} \cdot \mathbf{b} \rangle$.) Another problem is that when solving numerically the evolution equation for a space-dependent α-effect one needs for reasons of numerical stability a diffusion term [72,73]. However, it is now clear that a loss or exchange of small-scale helicity leads to an enhancement of the large-scale field [56], but from simulations we know that the presence of an equator rather lowers the energy of the mean field. Perhaps this could be fixed by adopting an additional loss term in the mean-field equation for the large-scale field, but this procedure would be completely ad hoc. One may hope however that some kind of a generalization of the dynamical α-quenching is at least in principle possible.

8 Conclusions

In this review we have outlined some of the main results of isotropic MHD simulations in the presence of helicity. We have focussed on the connection with the α-effect in mean-field dynamo theory. We should emphasize that in the case where the magnetic energy density is uniform in space, the agreement between simulations and theory is now well established. In all other cases, things are immediately more complicated. Moreover, dynamical quenching cannot readily be

generalized to the case where $\alpha_{\rm M}$ varies in space. In that case the equation for the magnetic helicity density would not be gauge-invariant. Another problem arises when $\alpha_{\rm K}$ varies in space and if it changes sign across the equator, for example. These are very important aspects requiring clarification. It is quite possible that significant improvement in the theory will soon be possible. Without a corresponding generalization of dynamic α-quenching, if it is ever possible, it would be difficult to use dynamo theory in astrophysically interesting circumstances.

References

1. E. N. Parker: Astrophys. J. 122, 293 (1955)
2. M. Steenbeck, F. Krause, K.-H. Rädler: Z. Naturforsch. 21a, 369 (1966) See also the translation in Roberts & Stix, "The turbulent dynamo" Tech. Note 60, NCAR, Boulder, Colorado (1971)
3. R. B. Leighton: Astrophys. J. 156, 1 (1969)
4. A. Ferriz-Mas, D. Schmitt, M. Schüssler: Astron. Astrophys. 289, 949 (1994)
5. A. Brandenburg, D. Schmitt: Astron. Astrophys. 338, L55 (1998)
6. A. Brandenburg, Å. Nordlund, R. F. Stein, U. Torkelsson: Astrophys. J. 446, 741 (1995)
7. A. Brandenburg, K. J. Donner: Month. Not. Roy. Astron. Soc. 288, L29 (1997)
8. P. A. Gilman, P. A. Fox: Astrophys. J. 484, 439 (1997)
9. F. Krause, K.-H. Rädler: *Mean-Field Magnetohydrodynamics and Dynamo Theory* (Akademie-Verlag, Berlin; also Pergamon Press, Oxford 1980)
10. A. Brandenburg: 'Disc Turbulence and Viscosity'. In: *Theory of Black Hole Accretion Discs*, ed. by M. A. Abramowicz, G. Björnsson & J. E. Pringle (Cambridge University Press 1998) pp. 61-86
11. G. Rüdiger, V. V. Pipin: Astron. Astrophys. 362, 756 (2000)
12. M. Steenbeck, F. Krause: Astron. Nachr. 291, 49 (1969)
13. G. Rüdiger, A. Brandenburg: Astron. Astrophys. 296, 557 (1995)
14. M. Dikpati, P. Charbonneau: Astrophys. J. 518, 508 (1999)
15. M. Küker, G. Rüdiger, M. Schultz: Astron. Astrophys. 374, 301 (2001)
16. F. Cattaneo: Astrophys. J. 515, L39 (1999)
17. E. T. Vishniac, J. Cho: Astrophys. J. 550, 752 (2001)
18. R. Arlt, A. Brandenburg: Astron. Astrophys. 380, 359 (2001)
19. A. Brandenburg: Astrophys. J. 550, 824 (2001a)
20. A. Brandenburg, W. Dobler: Astron. Astrophys. 369, 329 (2001)
21. E. G. Blackman, G. F. Field: Astrophys. J. 534, 984 (2000)
22. N. I. Kleeorin, D. Moss, I. Rogachevskii, D. Sokoloff: Astron. Astrophys. 361, L5 (2000)
23. A. Brandenburg, W. Dobler, K. Subramanian: Astron. Nachr. 323, 99 (2002)
24. N. Seehafer: Solar Phys. 125, 219 (1990)
25. A. A. Pevtsov, R. C. Canfield, T. R. Metcalf: Astrophys. J. 440, L109 (1995)
26. S. D. Bao, H. Q. Zhang, G. X. Ai, M. Zhang: Astron. Astrophys. 139, 311 (1999)
27. A. A. Pevtsov, S. M. Latushko: Astrophys. J. 528, 999 (2000)
28. M. A. Berger, A. Ruzmaikin: J. Geophys. Res. 105, 10481 (2000)
29. C. R. DeVore: Astrophys. J. 539, 944 (2000)
30. J. Chae: Astrophys. J. 540, L115 (2000)
31. B. C. Low: J. Geophys. Res. 106, 25,141 (2001)

32. A. Brandenburg, Å. Nordlund, P. Pulkkinen, R. F. Stein, I. Tuominen: Astron. Astrophys. 232, 277 (1990)
33. K. Ferrière: Astrophys. J. 389, 286 (1992)
34. G. Rüdiger, L. L. Kitchatinov: Astron. Astrophys. 269, 581 (1993)
35. M. Ossendrijver, M. Stix, A. Brandenburg: Astron. Astrophys. 376, 713 (2001)
36. A. Brandenburg: astro-ph/0109497 (2001)
37. M. Meneguzzi, U. Frisch, A. Pouquet: Phys. Rev. Lett. 47, 1060 (1981)
38. B. Galanti, P.-L. Sulem: Phys. Fluids A 3, 1778 (1991)
39. B. Galanti, P.-L. Sulem, A. D. Gilbert: Physica D 47, 416 (1991)
40. D. Balsara, A. Pouquet: Phys. Plasmas 6, 89 (1999)
41. A. D. Gilbert: Geophys. Astrophys. Fluid Dyn. 96, 135 (2002)
42. D. W. Hughes, F. Cattaneo, E. J. Kim: Phys. Lett. 223, 167 (1996)
43. M. Berger, G. B. Field: J. Fluid Mech. 147, 133 (1984)
44. A. Brandenburg, G. R. Sarson: Phys. Rev. Lett. 88, 055003 (2002)
45. G. A. Glatzmaier, P. H. Roberts: Nature 377, 203 (1995)
46. A. Pouquet, U. Frisch, J. Léorat: J. Fluid Mech. 77, 321 (1976)
47. A. Brandenburg, D. Sokoloff: Geophys. Astrophys. Fluid Dyn., in press (2002), astro-ph/0111568
48. M. Berger: Geophys. Astrophys. Fluid Dyn. 30, 79 (1984)
49. M. R. Brown, R. C. Canfield, A. A. Pevtsov: *Magnetic Helicity in Space and Laboratory Plasmas* (Geophys. Monograph **111**, American Geophysical Union, Florida 1999)
50. M. Dikpati, P. A. Gilman: Astrophys. J. 559, 428 (2001)
51. B. R. Durney: Solar Phys. 166, 231 (1995)
52. A. R. Choudhuri, M. Schüssler, M. Dikpati: Astron. Astrophys. 303, L29 (1995)
53. F. Cattaneo, S. I. Vainshtein: Astrophys. J. 376, L21 (1991)
54. S. I. Vainshtein, F. Cattaneo: Astrophys. J. 393, 165 (1992)
55. F. Cattaneo, D. W. Hughes: Phys. Rev. E 54, R4532 (1996)
56. E. G. Blackman, A. Brandenburg: Astrophys. J., in press (2002), astro-ph/0204497
57. G. B. Field, E. G. Blackman, H. Chou: Astrophys. J. 513, 638 (1999)
58. A. Brandenburg, A. Bigazzi, K. Subramanian: Month. Not. Roy. Astron. Soc. 325, 685 (2001)
59. A. V. Gruzinov, P. H. Diamond: Phys. Rev. Lett. 72, 1651 (1994)
60. A. V. Gruzinov, P. H. Diamond: Phys. Plasmas 2, 1941 (1995)
61. A. V. Gruzinov, P. H. Diamond: Phys. Plasmas 3, 1853 (1996)
62. A. Bhattacharjee, Y. Yuan: Astrophys. J. 449, 739 (1995)
63. A. Brandenburg: 'Helicity in large-scale dynamo simulations'. In: *Magnetic Helicity in Space and Laboratory Plasmas*, ed. by M. R. Brown, R. C. Canfield, A. A. Pevtsov (Geophys. Monograph **111**, American Geophysical Union, Florida 1999) pp. 65-73
64. G. B. Field, E. G. Blackman: Astrophys. J. 572, 685 (2002)
65. N. I. Kleeorin, A. A. Ruzmaikin: Magnetohydrodynamics 18, 116 (1982); translation from Magnitnaya Gidrodinamika, 2, pp. 17–24 (1982)
66. Ya. B. Zeldovich, A. A. Ruzmaikin, D. D. Sokoloff: *Magnetic Fields in Astrophysics* (Gordon & Breach, New York 1983)
67. N. I. Kleeorin, I. Rogachevskii, A. Ruzmaikin: Astron. Astrophys. 297, 159 (1995)
68. A. A. Ruzmaikin: Comments Astrophys. 9, 85 (1981)
69. S. Schmalz, M. Stix: Astron. Astrophys. 245, 654 (1991)
70. U. Feudel, W. Jansen, J. Kurths: J. Bifurcation & Chaos 3, 131 (1993)
71. E. Covas, A. Tworkowski, A., Brandenburg, R. Tavakol: Astron. Astrophys. 317, 610 (1997)

72. N. I Kleeorin, D. Moss, I. Rogachevskii, D. Sokoloff: Astron. Astrophys. 387, 453 (2002)
73. E. Covas, R. Tavakol, A. Tworkowski, A. Brandenburg: Astron. Astrophys. 329, 350 (1998)